Fang et al. Nanoscale Research Letters (2015) 10:68
DOI 10.1186/s11671-014-0714-1

Nanoscale Research Letters
a SpringerOpen Journal

NANO EXPRESS Open Access

Stepwise mechanism and H_2O-assisted hydrolysis in atomic layer deposition of SiO_2 without a catalyst

Guo-Yong Fang[1,2*], Li-Na Xu[2], Lai-Guo Wang[1], Yan-Qiang Cao[1], Di Wu[1] and Ai-Dong Li[1*]

Abstract

Atomic layer deposition (ALD) is a powerful deposition technique for constructing uniform, conformal, and ultrathin films in microelectronics, photovoltaics, catalysis, energy storage, and conversion. The possible pathways for silicon dioxide (SiO_2) ALD using silicon tetrachloride ($SiCl_4$) and water (H_2O) without a catalyst have been investigated by means of density functional theory calculations. The results show that the $SiCl_4$ half-reaction is a rate-determining step of SiO_2 ALD. It may proceed through a stepwise pathway, first forming a Si-O bond and then breaking Si-Cl/O-H bonds and forming a H-Cl bond. The H_2O half-reaction may undergo hydrolysis and condensation processes, which are similar to conventional SiO_2 chemical vapor deposition (CVD). In the H_2O half-reaction, there are massive H_2O molecules adsorbed on the surface, which can result in H_2O-assisted hydrolysis of the Cl-terminated surface and accelerate the H_2O half-reaction. These findings may be used to improve methods for the preparation of SiO_2 ALD and H_2O-based ALD of other oxides, such as Al_2O_3, TiO_2, ZrO_2, and HfO_2.

Keywords: Silicon dioxide; Atomic layer deposition; H_2O-assisted hydrolysis

Background

Atomic layer deposition (ALD) is a powerful deposition technique for constructing uniform, conformal, and ultrathin films in microelectronics, photovoltaics, catalysis, energy storage, and conversion [1,2]. Compared to other fabrication techniques, such as physical vapor deposition (PVD) and chemical vapor deposition (CVD), ALD is capable of accurately controlling the thickness of thin films at the atomic scale [1]. Essentially, the principle of ALD is similar to that of CVD, except that ALD breaks the CVD reaction into two half-reactions and retains two precursors separately during the reaction [2]. Taking silicon dioxide (SiO_2) as an example, SiO_2 CVD using silicon tetrachloride ($SiCl_4$) and water (H_2O) can be divided into two half-reactions, A and B, of SiO_2 ALD [3-6]:

$$\mathrm{CVD}: \mathrm{SiCl_4} + 2\mathrm{H_2O} \rightarrow \mathrm{SiO_2} + 4\mathrm{HCl},$$
$$\mathrm{ALD}: (\mathrm{A})\ \mathrm{Si\text{-}OH^*} + \mathrm{SiCl_4} \rightarrow \mathrm{Si\text{-}O\text{-}SiCl_3^*} + \mathrm{HCl},$$
$$(\mathrm{B})\ \mathrm{Si\text{-}O\text{-}SiCl^*} + \mathrm{H_2O} \rightarrow \mathrm{Si\text{-}O\text{-}Si\text{-}OH^*} + \mathrm{HCl},$$

where an asterisk designates the surface species.

In order to get more insight into the reaction mechanism of SiO_2 ALD, theoretical calculation has been performed that illustrates the reaction pathways [7]. It was proposed that on the Si(001) surface, the substituted half-reaction of $SiCl_4$ with surface hydroxyl group (–OH) proceeds through a concerted pathway via a four-membered ring (4MR) transition state (TS), forming Si-O and H-Cl bonds while simultaneously breaking Si-Cl and O-H bonds [7]. Unlike the Lewis acids, such as $AlCl_3$, $TiCl_4$, $ZrCl_4$, and $HfCl_4$, however, $SiCl_4$ seems to have no strong nucleophilicity [8-10]. Furthermore, it was found experimentally that the rate-determining step (RDS) of the full cycle of SiO_2 ALD is the $SiCl_4$ half-reaction, not the H_2O half-reaction [3-6]. To date, the reaction mechanism of the full SiO_2 ALD process on the actual SiO_2 surface has remained unclear. In this work, we have performed detailed density functional theory (DFT) calculations to investigate the reaction mechanism of the full cycle of SiO_2 ALD, involving the $SiCl_4$ half-reaction (A1 and A2) and H_2O half-reaction (B1 to B10), as shown in Figure 1. It is demonstrated that the $SiCl_4$ half-reaction may undergo a stepwise pathway and H_2O can accelerate the H_2O half-reaction. The insights gained into the reaction mechanism of SiO_2 ALD may be used to improve methods for SiO_2

* Correspondence: fanggy@wzu.edu.cn; adli@nju.edu.cn
[1]National Laboratory of Solid State Microstructures, College of Engineering and Applied Sciences, Collaborative Innovation Center of Advanced Microstructures, Nanjing University, Nanjing 210093, China
[2]Zhejiang Provincial Key Laboratory of Carbon Materials, College of Chemistry and Materials Engineering, Wenzhou University, Wenzhou 325035, China

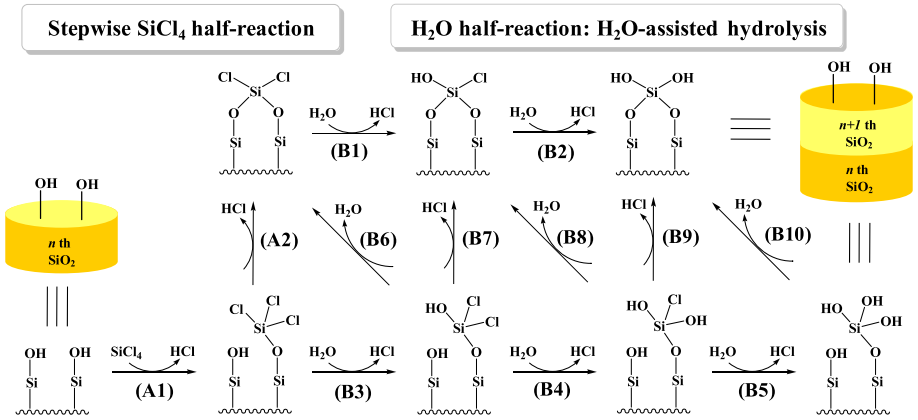

Figure 1 Possible reaction mechanism of the full ALD cycle of SiO_2 using $SiCl_4$ and H_2O. *n* represents ALD cycles.

ALD and H_2O-based ALD of other oxides, such as Al_2O_3, TiO_2, ZrO_2, and HfO_2.

Methods

In order to model the two half-reactions of SiO_2 ALD, we adopt the cluster model $Si_{23}O_{40}H_{40}$, as shown in Figure 2, which is based on a hydroxylated α-SiO_2(0001) surface. The cluster model consists of three layers of SiO_2 ($Si_{23}O_{40}$), and 40 hydrogen atoms which are used to saturate the dangling bonds. To stimulate the surface, the lower two layers of the SiO_2 atoms of the two models were fixed in optimized geometries.

All the species in ALD SiO_2 reactions were optimized using the M06-2X functional within the framework of DFT [11,12]. In order to gain a compromise between accuracy and computational cost, the 6-31G basis set was used for the fixed atoms of the substrate and the 6-31G(d, p) basis set was employed for other atoms on the surface. For each stationary point on the potential energy surface, a frequency calculation was carried out to determine if it is a minimum or a TS. All the transition states were verified by intrinsic reaction coordinates (IRC) calculations. Gibbs free energies of all species were estimated from the partition functions, and the enthalpy and entropy terms at 600 K. The energies reported here include zero-point energy (ZPE) corrections. We note that the solid surface lacks translational and rotational freedom, and the entropy of the surface only has a vibrational contribution. In other words, after being adsorbed onto the surface, the gas molecules lose translational and rotational momenta and produce new vibrational modes. All calculations in this work were performed with Gaussian 09 program [13].

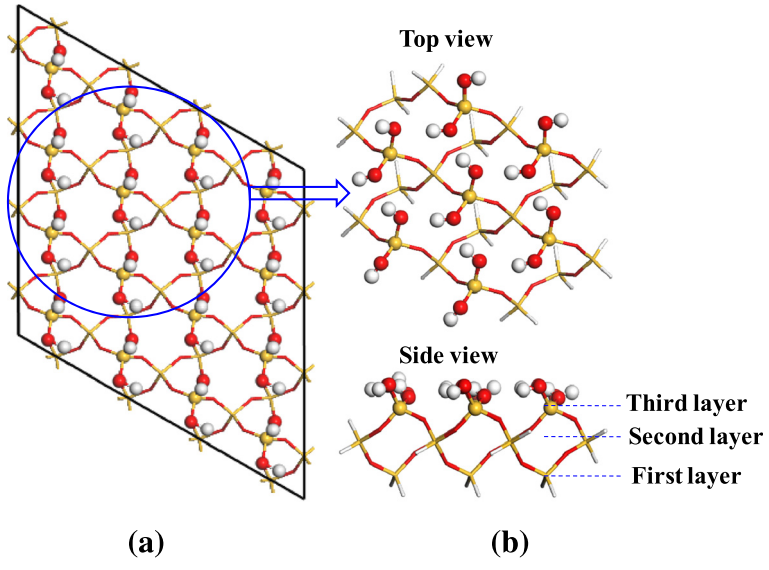

Figure 2 SiO_2 (0001) surface (a) and cluster model $Si_{23}O_{40}H_{40}$ (b).

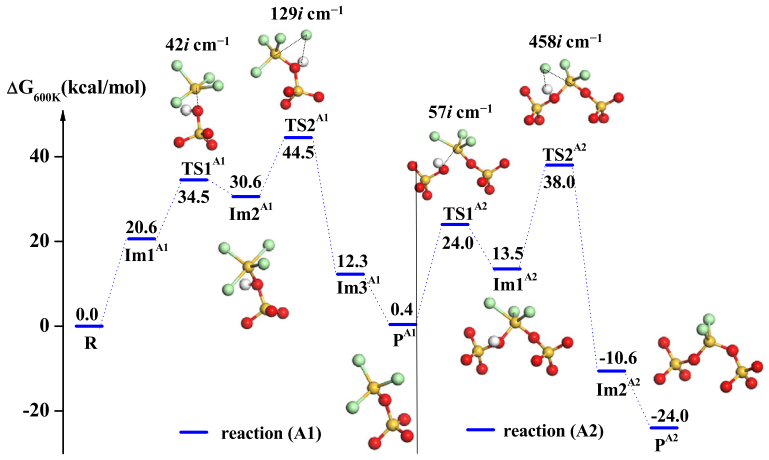

Figure 3 Gibbs free energy profile of the $SiCl_4$ half-reaction of SiO_2 ALD. The inset shows the structures of four transition states, $TS1^{A1}$, $TS2^{A1}$, $TS1^{A2}$, and $TS2^{A2}$, two pentacoordinated intermediates, $Im2^{A1}$ and $Im1^{A2}$, and two products, P^{A1} and P^{A2}.

Results and discussion

$SiCl_4$ half-reaction: stepwise mechanism

The reaction pathway for the $SiCl_4$ half-reaction between $SiCl_4$ precursor and the surface hydroxyl (-OH) is shown in Figure 3. Due to high levels of hydroxyls on the SiO_2 surface after H_2O half-reaction, $SiCl_4$ and hydroxyl may exchange ligands twice in the $SiCl_4$ half-reaction. Firstly, reaction A1 between $SiCl_4$ and -OH goes through a rotation transition state, $TS1^{A1}$, with a Gibbs free energy barrier (G_a) of 34.5 kcal mol^{-1} and forms a pentacoordinated intermediate, $Im2^{A1}$. Subsequently, the unstable intermediate undergoes the second transition state, $TS2^{A1}$, forming the product $-OSiCl_3^*$, P^{A1} and accompanied by the release of HCl. Secondly, $-OSiCl_3$ can further react with another adjacent hydroxyl (-OH) on the surface to form the bridged product $-O_2SiCl_2^*$, P^{A2}. Similar to reaction A1, reaction A2 between $-OSiCl_3^*$ and -OH also undergoes two transition states, $TS1^{A2}$ and $TS2^{A2}$, and a pentacoordinated intermediate, $Im1^{A2}$. The overall $SiCl_4$ half-reaction is exergonic by 24.0 kcal mol^{-1}. The highest activation free energy of the $SiCl_4$ half-reaction is 44.5 kcal mol^{-1} ($TS2^{A1}$), indicating that the $SiCl_4$ half-reaction is very difficult. This difficulty can be overcome by the introduction of Lewis base catalysts, such as ammonia, pyridine, and aminosilane [14-22].

In Figure 3, $TS1^{A1}$ and $TS1^{A2}$, with imaginary frequencies of 42*i* and 57*i* cm^{-1}, respectively, represent the formation of a Si-O bond accompanied by the rotation of $SiCl_4$ and $-SiCl_3$. The pentacoordinated intermediates, $Im2^{A1}$ and $Im1^{A2}$, have a trigonal bipyramidal (TBP) geometry with five ligands of four Cl atoms and one O atom or three Cl atoms and two O atoms. The $TS2^{A1}$ and $TS2^{A2}$, with imaginary frequencies of 129*i* and 458*i* cm^{-1}, respectively, represent cleavages of the Si-Cl and O-H bonds and the formation of a H-Cl bond. As listed in Table 1, the Si···O and H···Cl distances in reaction A1 gradually decrease from 2.01 and 2.62 Å to 1.62 and 1.29 Å, respectively, indicating the formation of new Si-O and H-Cl bonds. Simultaneously, the O-H and Si-Cl distances increase from 1.03 and 2.11 Å to 4.86 and 4.88 Å, respectively, indicating cleavage of old O-H and Si-Cl bonds. Similar to reaction A1, the Si···O and H···Cl distances in reaction A2 gradually decrease from 2.95 and 3.81 Å to 1.62 and 1.29 Å, respectively, indicating the formation of new Si-O and H-Cl bonds. Simultaneously, the O-H and Si-Cl distances increase from 0.97 and 2.05 Å to 3.44 and 4.02 Å, respectively, indicating the cleavage of these bonds.

H_2O half-reaction: H_2O-assisted hydrolysis

In conventional SiO_2 CVD, $SiCl_4$ and H_2O are introduced into the reaction chamber simultaneously. Subsequent hydrolysis and condensation lead to the formation of SiO_2. Although two reactants are separately introduced into the chamber, hydrolysis and condensation also occur in SiO_2 ALD. In fact, the half-reaction between water and the Cl-terminated surface exchanges Cl

Table 1 Selected bond distances (in Å) of all species for $SiCl_4$ half-reaction

Species	Si-O	O-H	Si-Cl	H-Cl
$Im1^{A1}$	2.01	1.03	2.11	2.62
$TS1^{A1}$	1.83	1.08	2.24	2.83
$Im2^{A1}$	1.79	1.13	2.24	3.21
$TS2^{A1}$	1.77	1.02	2.94	2.01
$Im3^{A1}$	1.62	4.86	4.88	1.29
P^{A1}	2.95	0.97	2.05	3.81
$TS1^{A2}$	2.10	1.00	2.11	2.95
$Im1^{A2}$	1.83	1.02	2.27	2.76
$TS2^{A2}$	1.79	1.14	2.50	1.65
$Im2^{A2}$	1.62	3.44	4.02	1.29

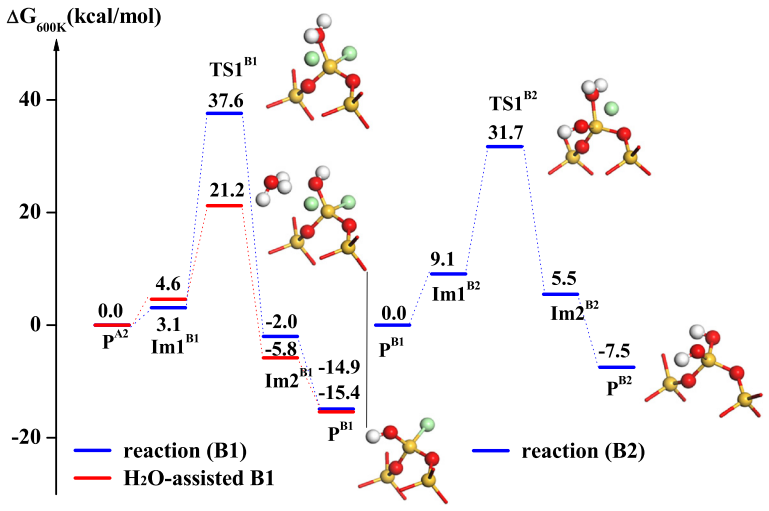

Figure 4 Gibbs free energy profiles of the hydrolysis reactions of -$O_2SiCl_2^*$, B1 and B2, in H_2O half-reaction. The inset shows the structures of three transition states, $TS1^{B1}$, $TS1^{B2}$, and H_2O-assisted-$TS1^{B1}$, and two products, P^{B1} and P^{B2}.

and -OH ligands and changes Si-Cl* species into Si-OH* species. Due to this the possible reactions of the H_2O half-reaction (B) may include the formation of silanol (-Si-OH) via the exchange of ligands between Cl and -OH (reactions B1, B2, B3, B4, and B5) and the formation of -O-Si-O- bridge bonds by removing H_2O (reactions B6, B8, and B10) and HCl (reactions B7 and B9), similar to the hydrolysis (-Si-OH) and condensation (-O-Si-O-) processes of SiO_2 CVD.

After the $SiCl_4$ half-reaction, the hydroxylated surface is terminated by Cl atoms and changes to -$O_2SiCl_2^*$ and -$OSiCl_3^*$ surfaces, which are both hydrolyzed in subsequent H_2O half-reaction. Firstly, H_2O and the bridged surface (-$O_2SiCl_2^*$) can exchange the ligands via reactions B1 and B2, shown in Figure 4. The first Cl exchange of the hydrolysis of -$O_2SiCl_2^*$ requires a high activation free energy of 37.6 kcal mol^{-1} and goes through a transition state, $TS1^{B1}$, to form -Si-OH* species and release HCl from the surface. Subsequently, the second Cl atom of -$O_2SiCl_2^*$ can also be exchanged by -OH via a transition state, $TS1^{B2}$, with an activation free energy of 31.7 kcal mol^{-1}. If H_2O-assisted role is considered, the activation free energy of the hydrolysis of -$O_2SiCl_2^*$ decreases to approximately 21.2 kcal mol^{-1}, indicating that H_2O can accelerate -Si-OH formation and Cl elimination. The reason for this is mainly that H_2O can form hydrogen bonding interactions through H_2O…H_2O bonds and lower the activation energy of Si-O bond formation and Cl elimination via a six-member ring (6MR) transition state, H_2O-assisted-$TS1^{B1}$, shown in Figure 4. The accelerated

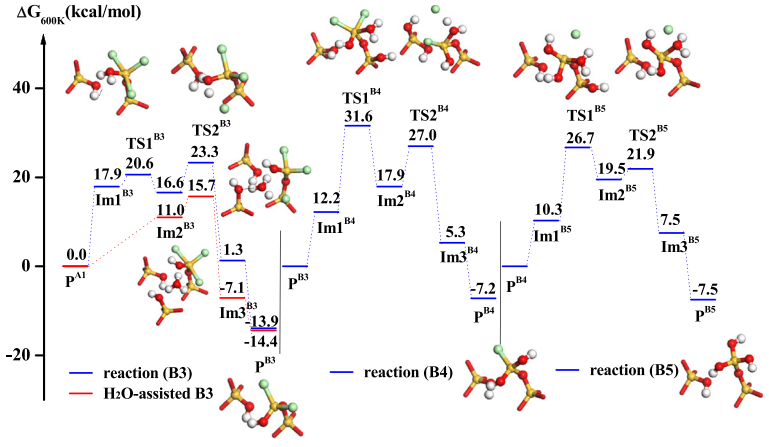

Figure 5 Gibbs free energy profiles of the hydrolysis reactions of -$OSiCl_3^*$, B3, B4, and B5, in H_2O half-reaction. The inset shows the structures of seven transition states, $TS1^{B3}$, $TS2^{B3}$, $TS1^{B4}$, $TS2^{B4}$, $TS1^{B5}$, $TS2^{B5}$, and H_2O-assisted-$TS2^{B3}$, a pentacoordinated intermediate, H_2O-assisted-$Im2^{B3}$, and three products, P^{B3}, P^{B4}, and P^{B5}.

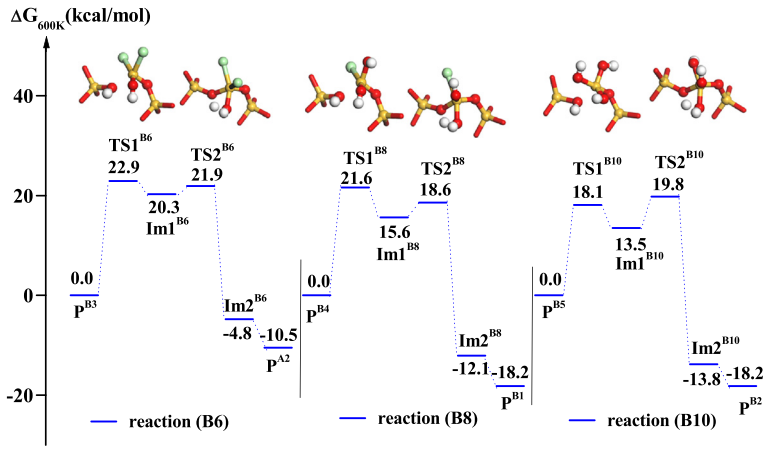

Figure 6 Gibbs free energy profiles of H_2O condensation reactions, B6, B8, and B10, in H_2O half-reaction. The inset shows the structures of six transition states, $TS1^{B6}$, $TS2^{B6}$, $TS1^{B8}$, $TS2^{B8}$, $TS1^{B10}$, and $TS2^{B10}$.

half-reaction via the hydrogen bonding interaction of $H_2O…H_2O$ may be termed as H_2O-assisted hydrolysis, which is similar to Lewis-base catalysis in SiO_2 ALD through the OH…N hydrogen bond [14,23,24]. As a matter of fact, there are H_2O-assisted reactions in nature, such as hydrolysis or solvolysis [25-28], tautomerization or proton transfer [29-34], decomposition [35-37], and catalysis [38,39]. H_2O-assisted hydrolysis and solvolysis facilitate the exchange and dissociation of Cl ligand in HfO_2 ALD using $HfCl_4$ and H_2O [40].

Secondly, another Cl-terminated surface (-$OSiCl_3^*$) can also hydrolyze step-by-step and go through pathways, B3, B4, and B5, shown in Figure 5. Three ligand exchange reactions undergo two transition states, $TS1^{B3}$ and $TS2^{B3}$, $TS1^{B4}$ and $TS2^{B4}$, and $TS1^{B5}$ and $TS2^{B5}$. Similar to the $SiCl_4$ half-reaction, the first represents the formation of Si-O bonds and the second represents the cleavages of Si-Cl and O-H bonds and the formation of H-Cl bond. It is found that the activation free energies of -$OSiCl_3^*$ hydrolysis are lower than that of -$O_2SiCl_2^*$ hydrolysis. Unlike the rigid -O_2SiCl_2 group, the -$OSiCl_3$ group is more flexible. As shown in $TS1^{B3}$ of Figure 5, the hydroxyl (-OH) on the surface can interact with H_2O through hydrogen bonding, HOH…OH, and cause the rotation of the -$OSiCl_3$ group, which can accelerate the hydrolysis of -$OSiCl_3$ and H_2O exchange with the Cl ligand. The first hydrolysis of -$OSiCl_3^*$ requires a low activation free energy of 23.3 kcal mol^{-1}; however, the hydrolysis of -$OSiOH\text{-}Cl_2^*$ and -$OSi(OH)_2\text{-}Cl^*$ require slightly higher activation free energies. The reason for this may be that the direction of the hydrolyzed Cl atom of -$OSiCl_3^*$ is more downward than that of -$OSiOH\text{-}Cl_2^*$ or -$OSi(OH)_2\text{-}Cl^*$, which results in a hydrogen bonding interaction between -OH and H_2O. In the H_2O half-reaction, there are massive H_2O molecules adsorbed on the surface, which result in H_2O-assisted hydrolysis. Owing to the strong hydrogen bonding interaction of $H_2O\cdots H_2O$, a pentacoordinated intermediate including silanol (Si-OH) ligand can be directly formed, as shown in H_2O-assisted $Im2^{B3}$ in Figure 5. The hydrolysis of -$OSiCl_3^*$ and the elimination of Cl ligand occur easily and the activation free energy can decrease from 23.3 to 15.0 kcal mol^{-1}. Similarly, H_2O can also accelerate the hydrolysis of -$OSiOH\text{-}Cl_2^*$ and -$OSi(OH)_2\text{-}Cl^*$.

As show in Figure 6, the formation of the O-Si-O bridge bond can result from H_2O condensation reactions, B6, B8, and B10, similar to the condensation (O-Si-O) process of SiO_2 CVD. These condensation reactions occur after the hydrolysis of -$OSiCl_3^*$, -$OSiOH\text{-}Cl_2^*$ and -$OSi(OH)_2\text{-}Cl^*$ and include two transition states. The first transition states, $TS1^{B6}$, $TS1^{B8}$, and $TS1^{B10}$, represent O-Si-O bond formation with the activation free energies of 22.9, 21.6,

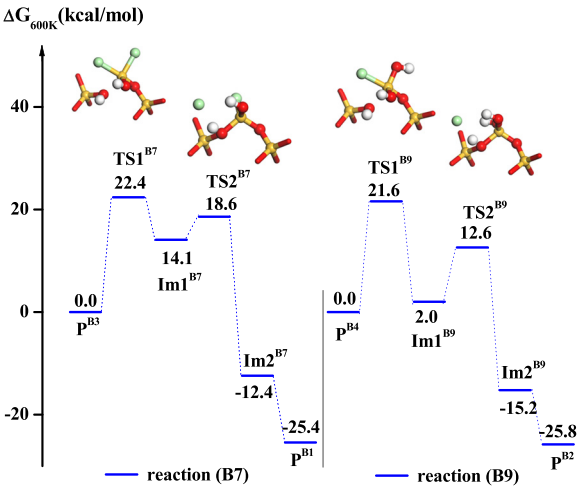

Figure 7 The Gibbs free energy profiles of HCl condensation reactions, B7 and B9, in H_2O half-reaction. The inset shows the structures of four transition states, $TS1^{B7}$, $TS2^{B7}$, $TS1^{B9}$, and $TS2^{B9}$.

and 18.1 kcal mol^{-1}, respectively. The second transition states, $TS2^{B6}$, $TS2^{B8}$, and $TS2^{B10}$, represent H_2O removal with the activation free energies of 21.9, 18.6, and 19.8 kcal mol^{-1}, respectively.

Similar to H_2O condensation, HCl condensation reactions, B7 and B9, can also result in the formation of the O-Si-O bridge bond with low activation free energies of 22.4 and 21.6 kcal mol^{-1}, respectively, as show in Figure 7. The corresponding activation free energies of HCl removal are 18.6 and 12.6 kcal mol^{-1}, respectively. During H_2O or HCl removal, the two condensations both lead to the formation of the O-Si-O bridge bond, which is the elementary unit of SiO_2 and ensures its ALD growth.

When reviewing the full SiO_2 ALD cycle, including reactions A1 to A2 and B1 to B10, we find that the free energy barrier for the H_2O half-reaction is lower than that for $SiCl_4$ half-reaction. The principal reason is that there are massive H_2O molecules adsorbed on the surface, which result in H_2O-assisted hydrolysis of $-O_2Si-Cl_2^*$, $-O_2SiOH-Cl^*$, $-OSi-Cl_3^*$, $-OSiOH-Cl_2^*$, and $-OSi(OH)_2-Cl^*$ and accelerate the H_2O half-reaction. Therefore, the $SiCl_4$ half-reaction is the RDS of the full ALD cycle of SiO_2 and controls the ALD growth of SiO_2.

Conclusions

Through detailed DFT calculations, the possible reaction pathways of (A) $SiCl_4$ half-reaction and (B) H_2O half-reaction in SiO_2 ALD without a catalyst have been investigated. The $SiCl_4$ half-reaction is the RDS of SiO_2 ALD. It may proceed through a stepwise pathway, first forming a Si-O bond and then breaking Si-Cl and O-H bonds and forming a H-Cl bond. The H_2O half-reaction is a complicated process, including hydrolysis and condensation. In the H_2O half-reaction, there are massive H_2O molecules adsorbed on the surface, which can result in H_2O-assisted hydrolysis of the Cl-terminated surface and accelerate the H_2O half-reaction. These findings may be used in SiO_2 ALD and H_2O-based ALD of other oxides, such as Al_2O_3, TiO_2, ZrO_2, and HfO_2.

Competing interests

The authors declare that they have no competing interests.

Authors' contributions

GYF and ADL proposed an idea to elucidate the mechanism of SiO_2 ALD. LNX, LGW, YQC, and DW participated in the calculations and helped in the data analysis. GYF and LNX wrote the paper. All authors read and approved the final manuscript.

Acknowledgements

This work was supported by the National Natural Science Foundation of China (51202107), the State Key Program for Basic Research of China (2015CB921203 and 2011CB922104), the China Postdoctoral Science Foundation (2014 M551556), Open Project of National Laboratory of Solid State Microstructures (M27009), and Zhejiang Provincial Natural Science Foundation of China (LY13B030005). ADL is also grateful for the support of the Doctoral Fund of the Ministry of Education of China (20120091110049) and the Priority Academic Program Development (PAPD) in Jiangsu Province. We thank the High Performance Computing Center of Nanjing University for providing the computing resources.

Received: 12 November 2014 Accepted: 23 December 2014
Published online: 18 February 2015

References

1. Doering R, Nishi Y. Handbook of semiconductor manufacturing technology. 2nd ed. Boca Raton: CRC; 2007.
2. Pinna N, Knez M. Atomic layer deposition of nanostructured materials. New York: Wiley-VCH; 2011.
3. George SM, Sneh O, Dillon AC, Wise ML, Ott AW, Okada LA, et al. Atomic layer controlled deposition of SiO_2 and Al_2O_3 using ABAB… binary reaction sequence chemistry. Appl Surf Sci. 1994;82–83:460–7.
4. Sneh O, Wise ML, Ott AW, Okada LA, George SM. Atomic layer growth of SiO_2 on Si(100) using $SiCl_4$ and H_2O in a binary reaction sequence. Surf Sci. 1995;334:135–52.
5. George SM, Ott AW, Klaus JW. Surface chemistry for atomic layer growth. J Phys Chem. 1996;100:13121–31.
6. Klaus JW, Ott AW, Johnson JM, George SM. Atomic layer controlled growth of SiO_2 films using binary reaction sequence chemistry. Appl Phys Lett. 1997;70:1092–4.
7. Kang JK, Musgrave CB. Mechanism of atomic layer deposition of SiO_2 on the silicon (100)-2 × 1 surface using $SiCl_4$ and H_2O as precursors. J Appl Phys. 2002;91:3408–14.
8. Ritala M, Kukli K, Rahtu A, Räisänen PI, Leskelä M, Sajavaara T, et al. Atomic layer deposition of oxide thin films with metal alkoxides as oxygen sources. Science. 2000;288:319–21.
9. Hausmann D, Becker J, Wang S, Gordon RG. Rapid vapor deposition of highly conformal silica nanolaminates. Science. 2002;298:402–6.
10. Fang G, Ma J. Rapid atomic layer deposition of silica nanolaminates: synergistic catalysis of Lewis/Brønsted acid sites and interfacial interactions. Nanoscale. 2013;5:11856–69.
11. Zhao Y, Truhlar DG. Density functionals with broad applicability in chemistry. Acc Chem Res. 2008;41:157–67.
12. Zhao Y, Truhlar DG. The M06 suite of density functionals for main group thermochemistry, thermochemical kinetics, noncovalent interactions, excited states, and transition elements: two new functionals and systematic testing of four M06-class functionals and 12 other functional. Theor Chem Acc. 2008;120:215–41.
13. Frisch MJ, Trucks GW, Schlegel HB, Scuseria GE, Robb MA, Cheeseman JR, et al. Gaussian 09. Revision B.02. Wallingford CT: Gaussian, Inc; 2009.
14. Klaus JW, Sneh O, George SM. Growth of SiO_2 at room temperature with the use of catalyzed sequential half reaction. Science. 1997;278:1934–6.
15. Klaus JW, Sneh O, Ott AW, George SM. Atomic layer deposition of SiO_2 using catalyzed and uncatalyzed self-limiting surface reactions. Surf Rev Lett. 1999;6:435–48.
16. Klaus JW, George SM. Atomic layer deposition of SiO_2 at room temperature using NH_3-catalyzed sequential surface reactions. Surf Sci. 2000;447:81–90.
17. Klaus JW, George SM. SiO_2 chemical vapor deposition at room temperature using $SiCl_4$ and H_2O with an NH_3 catalyst. J Electrochem Soc. 2000;147:2658–64.
18. Ferguson JD, Smith ER, Weimer AW, George SM. ALD of SiO_2 at room temperature using TEOS and H_2O with NH_3 as the catalyst. J Electrochem Soc. 2004;151:G528–35.
19. Du Y, Du X, George SM. SiO_2 film growth at low temperatures by catalyzed atomic layer deposition in a viscous flow reactor. Thin Sol Film. 2005;491:43–53.
20. Du Y, Du X, George SM. Mechanism of pyridine-catalyzed SiO_2 atomic layer deposition studied by Fourier transform infrared spectroscopy. J Phys Chem C. 2007;111:219–26.
21. Hatton B, Kitaev V, Perovic D, Ozin G, Aizenberg J. Low-temperature synthesis of nanoscale silica multilayers - atomic layer deposition in a test tube. J Mater Chem. 2010;20:6009–13.
22. Bachmann J, Zierold R, Chong YT, Hauert R, Sturm C, Schmidt-Grund R, et al. A practical, self-catalytic, atomic layer deposition of silicon dioxide. Angew Chem Int Ed. 2008;47:6177–9.
23. Fang G, Chen S, Li A, Ma J. Surface pseudorotation in Lewis-base-catalyzed atomic layer deposition of SiO_2: static transition state search and Born – Oppenheimer molecular dynamics simulation. J Phys Chem C. 2012;116:26436–48.

24. Fang GY, Xu LN, Cao YQ, Wang LG, Wu D, Li DL. Self-catalysis by aminosilanes and strong surface oxidation by O_2 plasma in plasma-enhanced atomic layer deposition of high-quality SiO_2. Chem Commun. 2015;51:1341–4.
25. Antonczak S, Ruiz-López MF, Rivail JL. Ab initio analysis of water-assisted reaction mechanisms in amide hydrolysis. J Am Chem Soc. 1994;116:3912–21.
26. Schmeer G, Sturm P. A quantum chemical approach to the water assisted neutral hydrolysis of ethyl acetate and its derivatives. Phys Chem Chem Phys. 1999;1:1025–30.
27. Tsuchida N, Satou H, Yamabe S. Reaction paths of the water-assisted solvolysis of N, N-dimethylformamide. J Phys Chem A. 2007;111:6296–303.
28. Gao JY, Zeng Y, Zhang CH, Xue Y. Theoretical studies on the water-assisted hydrolysis of N, N-dimethyl-N′-(2′,3′-dideoxy-3′-thiacytidine) formamidine with three water molecules. J Phys Chem A. 2009;113:325–31.
29. Bell RL, Truong TN. Primary and solvent kinetic isotope effects in the water-assisted tautomerization of formamidine: an ab initio direct dynamics study. J Phys Chem A. 1997;101:7802–8.
30. Gu J, Leszczynski J. A DFT study of the water-assisted intramolecular proton transfer in the tautomers of adenine. J Phys Chem A. 1999;103:2744–50.
31. Liu GX, Li ZS, Ding YH, Fu Q, Huang XR, Sun CC, et al. Water-assisted isomerization from linear propargylium (H_2CCCH^+) to cyclopropenylium(c-$C_3H_3^+$). J Phys Chem A. 2002;106:10415–22.
32. Balta B, Aviyente V. Solvent effects on glycine II. Water-assisted tautomerization. J Comput Chem. 2004;25:690–703.
33. Markova N, Enchev V, Timtcheva I. Oxo-hydroxy tautomerism of 5-fluorouracil: water-assisted proton transfer. J Phys Chem A. 2005;109:1981–8.
34. Michalkova A, Kosenkov D, Gorb L, Leszczynski J. Thermodynamics and kinetics of intramolecular water assisted proton transfer in Na^+-1-methylcytosine water complexes. J Phys Chem B. 2008;112:8624–33.
35. Aplincourt P, Anglada JM. Theoretical studies of the isoprene ozonolysis under tropospheric conditions. 2. Unimolecular and water-assisted decomposition of the r-hydroxy hydroperoxides. J Phys Chem A. 2003;107:5812–20.
36. Jacobs G, Patterson PM, Graham UM, Crawford AC, Dozier A, Davis BH. Catalytic links among the water–gas shift, water-assisted formic acid decomposition, and methanol steam reforming reactions over Pt-promoted thoria. J Cat. 2005;235:79–91.
37. Huang J, Yeung CS, Ma J, Gayner ER, Phillips DL. A computational chemistry investigation of the mechanism of the water-assisted decomposition of trichloroethylene oxide. J Phys Chem A. 2014;118:1557–67.
38. Ouchi M, Yoda H, Terashima T, Sawamoto M. Aqueous metal-catalyzed living radical polymerization: highly active water-assisted catalysis. Polym J. 2012;44:51–8.
39. Thorat PB, Goswami SV, Jadhav WN, Bhusare SR. Water-assisted organocatalysis: an enantioselective green protocol for the henry reaction. Aust J Chem. 2013;66:661–6.
40. Mukhopadhyay AB, Musgrave CB, Sanz JF. Atomic layer deposition of hafnium oxide from hafnium chloride and water. J Am Chem Soc. 2008;130:11996–2006.